



Layered double hydroxides derived Ni_x(Mg_yAl_zO_n) catalysts: Enhanced ammonia decomposition by hydrogen spillover effect



Qin Su^a, Lingli Gu^a, Yao Yao^a, Jing Zhao^a, Weijie Ji^{a,*}, Weiping Ding^a, Chak-Tong Au^b

^a Key Laboratory of Mesoscopic Chemistry, MOE, School of Chemistry and Chemical Engineering, Nanjing University, Nanjing 210093, China

^b Department of Chemistry, Hong Kong Baptist University, Kowloon Tong, Hong Kong

ARTICLE INFO

Article history:

Received 17 March 2016

Received in revised form 1 July 2016

Accepted 22 August 2016

Available online 24 August 2016

Keywords:

Layered double hydroxide

Ni-based catalyst

Ammonia

Decomposition

Hydrogen spillover

ABSTRACT

The NiMgAl-layered double hydroxides, with the stoichiometric ratios of Mg/Ni and Mg/Al being 0–9 and 0–3, respectively, were synthesized and employed as the Ni catalyst precursors for NH₃ decomposition. The resulting catalyst of the certain Ni, Mg, and Al contents showed high catalytic efficiency and outstanding durability for the target reaction. The features of cost effective (with only Mg and Al elements besides Ni), easy fabrication, and thermally durable are attractive for large-scale operation. The characterizations revealed the related changes in structure and property, such as the Ni particle size and distribution, the reduction of Ni²⁺ species, the Ni-oxide matrix interaction, the surface basicity as well as the adsorption/desorption behavior of hydrogen, in line with the stoichiometry of Ni, Mg, and Al in the samples. The superior catalytic activity and stability are thought to be associated with the structurally isolated active Ni species by the oxide matrix and the synergism between Ni-Mg sites. Particularly, the “spillover effect” of surface hydrogen accounts for a higher turnover frequency.

© 2016 Elsevier B.V. All rights reserved.

1. Introduction

Hydrogen is considered an ideal energy carrier which is widely used in various industrial processes. Technically, however, there are difficulties in storage and transportation of hydrogen due to its highly flammable, explosive, and low compressed characteristics, which limited its specific applications. Therefore, on-site generation of hydrogen by NH₃ decomposition has attracted extensive attention for easy handling and relatively low cost [1–3]. Furthermore, the ammonia decomposition process generates a solo by-product of nitrogen which is chemically inert, thus can satisfy the demand of proton-exchange membrane fuel cells (PEMFCs), meanwhile avoid the poisoning effect of cell electrodes by CO_x commonly existing in the hydrogen resources produced using carbonaceous raw material [1–5]. At present, the furnace for NH₃ decomposition is already commercially available, and has been used as a hydrogen protection atmosphere generator in some industrial processes, in order to replace the high energy consumed water electrolysis system. On account of the facts, the generation of hydrogen via NH₃ decomposition has been well accepted by research community and industry.

The synthesis of NH₃ is practically achieved so far through the well-known heterogeneous catalytic reaction [6,7], the detailed reaction mechanism is also helpful for studying the process of NH₃ decomposition. However, the good catalysts for NH₃ synthesis were found to be unsatisfactory for NH₃ decomposition owing to the differences in their surface reaction kinetics [7]. And because of this, many efforts have been devoted to developing the promising catalysts for NH₃ decomposition. Earlier studies on NH₃ decomposition mainly focused on the catalysts closely related to NH₃ synthesis/abatement in a diluted NH₃ atmosphere. In recent years, more research works employed pure NH₃ in reaction. For various materials tested in catalyzing pure NH₃ decomposition, it was recognized that the Ru-based catalysts showed superior performance among the noble metal ones, while the Ni-based catalysts were found to be better than other basic metal ones [3,4,8–10]. Since Ru is very costly especially when used in large scale, the Ni-based catalysts seem attractive to be an alternative choice. The activity of Ni catalyst can be enhanced by doping the rare earth elements such as La and Ce [11–13]. There were other structurally different Ni-based catalysts reported such as Ni/microfiber entrapped in Al₂O₃ [14], Ni/alumina-coated monoliths [15], in view of practical application. Although the Ni-based catalyst can be operated in large scale for NH₃ decomposition, efforts made in reducing catalyst cost, optimizing catalyst activity, and extending catalyst life never stop.

* Corresponding author.

E-mail address: jiwj@nju.edu.cn (W. Ji).

Layered double hydroxides (LDHs), represented by hydrotalcites, are a kind of layered anionic materials. It generally consists of replaceable positively charged mixed metal hydroxide layers and negatively charged interlayer anions [16], showing flexible physical and chemical properties. This kind of material has been employed as catalysts or catalyst precursors [17–20]. It was reported that Ni can be perfectly introduced into MgAl-LDHs to form NiMgAl-LDHs and the resulting NiMgAl mixed oxide have been used in a number of catalytic processes including reforming [21,22], hydrogenation [23], and dehydrogenation [24]. The mixed oxide obtained via calcination of the LDH precursor is characterized by the homogeneous inter-dispersion of all constituents [25–27]. Accordingly, Mg, Al, and Ni are highly distributed in the NiMgAl mixed oxide, showing excellent resistance to sintering because of the structural isolation by one another [28]. Besides, the presence of Mg can enhance the basicity of the resulting material [29–31]. The promotion effect of the basic site on a Ni-based catalyst for NH₃ decomposition was previously observed by Yin et al. [8]. Based on these unique features, one can envisage that a Ni catalyst derived from the precursor of NiMgAl-LDH is highly structure uniform, hence could be highly active and stable for the target reaction of NH₃ decomposition, and moreover, cost effective for practical application.

The aim of this work is therefore to develop the Ni-based catalysts by employing the NiMgAl-LDHs as the precursors in which the contents of Ni, Mg, and Al were systematically tuned. The effects of cation stoichiometry on phase structure, surface basicity, and catalytic behavior of the derived catalysts for NH₃ decomposition were elucidated through a series of physicochemical characterizations as well as performance evaluation. The results reveal that the generated Ni_x(Mg_yAl_zO_n) catalysts are easily made, highly efficient yet stable, even comparable with a Ru catalyst supported on Al₂O₃, a superb alternate among various Ni-based catalysts known for the target reaction. In particular, a spillover effect of surface hydrogen was found to be associated with the enhanced reaction on the basis of turnover frequency (**Scheme 1**).

2. Experimental

2.1. Catalyst preparation

NiMgAl-LDH precursors with different Ni, Mg, and Al stoichiometry were prepared according to the following procedures: certain amounts of Ni(NO₃)₂·6H₂O, Mg(NO₃)₂·6H₂O, and Al(NO₃)₃·9H₂O were dissolved in deionized water to make solution A (50 ml).

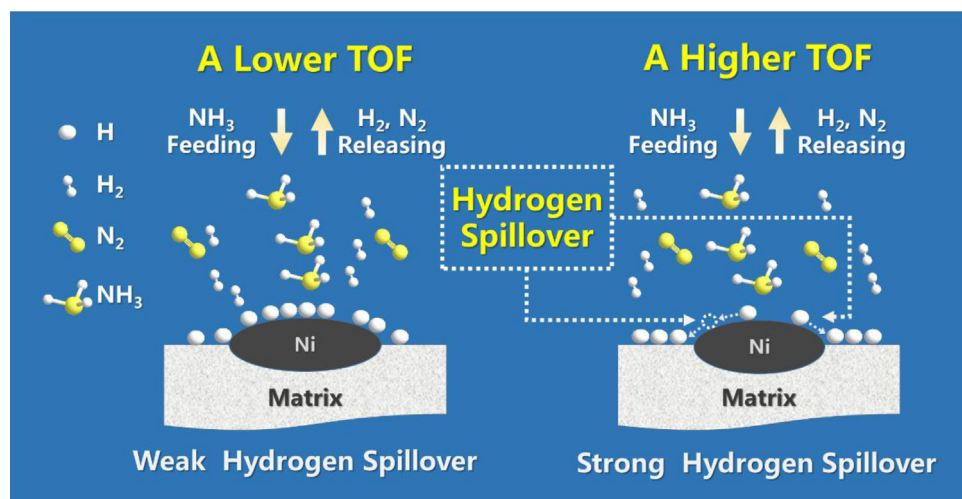
Separately, aqueous solution B (50 ml) was prepared, with the concentration of KOH and K₂CO₃ being 3 mol/l and 0.75 mol/l, respectively. Then solutions A and B were simultaneously added into a reaction vessel drop wise; and mixed with 10 ml deionized water upon stirring. The resulting mixture was continuously stirred at 323 K for 1 h, followed by a hydrothermal treatment at 373 K for 24 h. Finally, the precipitate was washed with deionized water and dried at 373 K overnight. After being calcined at 773 K for 6 h, the corresponding samples are labeled as Ni_xMg_yAl_zO_m in which x, y, and z stand for the molar concentration of Ni, Mg, and Al in solution A, respectively. That is to say, the Ni, Mg, and Al contents denoted in the sample series are the nominal values. In **Table 1**, the nominal and actual contents of Ni, Mg, and Al elements, the actual Ni content in weight percentage, as well as the actual Ni/Mg and Mg/Al molar ratios are presented. Based on the ICP measurement, the content of residual K in our samples looks rather limited (Table S1), and at this level of K content, the resulting effect on the Ni activity is minor (the promotion effect of K on Ru is more significant though) [3,8]. Moreover, the catalysts with the highest/lowest TOF values do not correspond to the highest or lowest K content in this study, which further suggests there is no direct correlation between the activity and the presence of residual K.

The catalysts were further *in situ* reduced by a 25% H₂/Ar flow at 973 K for 2 h, and then purged with pure Ar for activity evaluation. The reduced samples are denoted as Ni_x(Mg_yAl_zO_n). Note that the values of n and m could vary with the relative contents of Ni, Mg, and Al in the samples, but they are not specified in different cases. Ru/Al₂O₃ and K-Ru/Al₂O₃ (Ru loading = 5 wt.% with the Ru/K molar ratio = 2) were prepared by a modified method referred to the literature [8] using ethanol as solvent.

2.2. Catalyst characterization

The content of Ni, Mg, and Al was measured by ICP-AES on a J-A1100 Versa Probe spectrometer. X-ray diffraction (XRD) measurement was performed on a diffractometer (Rigaku Ultima IV) with Ni-filtered Cu K α radiation ($\lambda = 0.15405$ nm). Transmission electron microscopy (TEM) images were taken on an electron microscope (JEOL-1011) operated at 100 kV.

Temperature programmed reduction (TPR) was carried out in a quartz reactor connected to a thermal conductivity detector (TCD) under an atmosphere of 10% H₂/Ar. 25 mg of sample was used for each measurement. Before switched to the H₂/Ar stream, the sample was pretreated in a He stream at 773 K for 30 min. The TPR procedure started from 373 to 1123 K at a rate of 10 K/min, and hold



Scheme 1. The illustration of hydrogen spillover effect on the Ni_x(Mg_yAl_zO_n) catalysts.

Table 1

The nominal and actual content of Ni, Mg, and Al constituents in various catalysts.

Samples with nominal Ni/Mg/Al molar ratio	Ni/Mg/Al molar ratio determined by ICP	Ni wt.% determined by ICP	Actual Ni/Mg (Mg/Al) molar ratio
$\text{Ni}_{0.12}\text{Mg}_{1.08}\text{Al}_{0.3}\text{O}_n$	0.12/1.09/0.3	10.2	0.11 (3.63)
$\text{Ni}_{0.3}\text{Mg}_{0.9}\text{Al}_{0.3}\text{O}_n$	0.3/0.89/0.3	24.9	0.34 (2.97)
$\text{Ni}_{0.6}\text{Mg}_{0.6}\text{Al}_{0.3}\text{O}_n$	0.61/0.6/0.3	41.8	1.02 (2.00)
$\text{Ni}_{0.9}\text{Mg}_{0.3}\text{Al}_{0.3}\text{O}_n$	0.84/0.28/0.3	60.0	3.0 (0.93)
$\text{Ni}_{1.08}\text{Mg}_{0.12}\text{Al}_{0.3}\text{O}_n$	1.14/0.12/0.3	66.9	9.5 (0.40)
$\text{Ni}_{1.2}\text{Al}_{0.3}\text{O}_n$	1.26/-/0.3	71.4	Mg=0
$\text{Ni}_{0.6}\text{Al}_{0.9}\text{O}_n$	0.6/-/0.83	40.5	Mg=0
$\text{Ni}_{0.6}\text{Mg}_{0.3}\text{Al}_{0.6}\text{O}_n$	0.6/0.29/0.57	40.1	2.07 (0.51)
$\text{Ni}_{0.6}\text{Mg}_{0.45}\text{Al}_{0.45}\text{O}_n$	0.6/0.43/0.44	42.8	1.40 (0.98)
$\text{Ni}_{0.6}\text{Mg}_{0.68}\text{Al}_{0.23}\text{O}_n$	0.6/0.64/0.23	44.8	0.94 (2.78)

at 1123 K for 30 min. The water generated during the reduction was removed by a trap filled with 4A molecular sieve.

The active surface area of metallic Ni was determined by pulse H₂-chemisorption. Before measurement, the sample (100 mg) was reduced at 973 K for 2 h under a flow of 25% H₂/Ar, then cooled down to 673 K under a dehydrated and deoxygenated Ar flow (flow rate = 40 ml/min) and maintained at this temperature for 3 h. Pulse H₂-chemisorption were performed at 323 K by sequentially injecting a definite amount of pure H₂ until saturation, the H₂ consumption was measured with a TCD.

Hydrogen temperature programmed desorption (H₂-TPD) was performed followed by the saturation of H₂ pulse chemisorption at 323 K. The H₂ adsorption saturated at 373 K was also performed for comparison. The sample was purged with a dehydrated and deoxygenated Ar flow at 323 K for 30 min, then the temperature was raised to 873 K at a rate of 10 K/min.

Carbon dioxide temperature programmed desorption (CO₂-TPD) was carried out in a conventional setup. The sample pretreatment was identical to that adopted for H₂-pulse chemisorption. After adsorption of CO₂ at 373 K for 30 min, the sample was purged in a dehydrated and deoxygenated Ar flow for 1 h, and then heated to 873 K at a rate of 10 K/min in an Ar flow. The effluent gas was analyzed with a TCD.

2.3. Catalytic activity

Activity evaluation of samples was carried out in a fixed-bed quartz tube reactor (catalyst amount = 100 mg, 60–80 mesh) under pure NH₃ (atmospheric pressure; flow rate = 50 ml/min; GHSV = 30,000 ml h⁻¹ g_{cat}⁻¹). Prior to reaction, the catalysts were reduced in situ by a 25% H₂/Ar flow at 973 K for 2 h, then purged with pure Ar. The reaction temperature was in the 723–973 K range. Products were analyzed by an on-line gas chromatograph (GC-112A, Shanghai INESA Analytical Instrument Co., Ltd.) equipped with a TCD and a Poropak Q column. NH₃ conversion in a blank reactor was less than 1.0% at 823 K.

3. Results and discussion

3.1. Catalytic activity

The catalytic performance of $\text{Ni}_x(\text{Mg}_y\text{Al}_z\text{O}_n)$ was systematically tuned by two approaches: maintaining the total amount of Ni, Mg, and Al meanwhile changing the molar ratio of Ni/Mg as well as that of Mg/Al in $\text{Ni}_x(\text{Mg}_y\text{Al}_z\text{O}_n)$.

Fig. 1a shows the NH₃ conversions achieved at different temperatures over $\text{Ni}_x(\text{Mg}_y\text{Al}_z\text{O}_n)$ in which various Ni/Mg molar ratios were applied. NH₃ conversion increases with increasing reaction temperature, coincident with the endothermic reaction feature of NH₃ decomposition. In the 723–973 K range, the NH₃ conversion increases significantly as the Ni/Mg molar ratio is raised from 0.11 to 0.33, but varies only slightly at a higher Ni/Mg molar

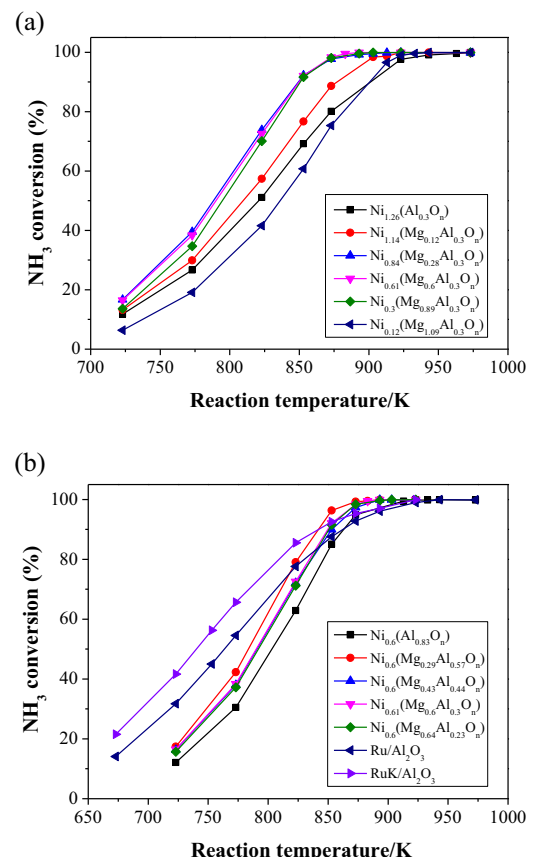


Fig. 1. NH₃ conversion as a function of reaction temperature over (a) $\text{Ni}_x(\text{Mg}_y\text{Al}_z\text{O}_n)$ with varied Ni/Mg molar ratio, and (b) $\text{Ni}_{0.6}(\text{Mg}_y\text{Al}_z\text{O}_n)$ with varied Mg/Al molar ratio. GHSV_{NH₃} = 30,000 ml h⁻¹ g_{cat}⁻¹, Ru loading = 5 wt.%.

ratio up to 3. Further increase in Ni/Mg ratio to 9 results in low NH₃ conversions. A complete replacement of Mg by Ni causes a lower conversion of NH₃. Full conversion can be obtained for all catalysts at about 950 K (Fig. 1). Moreover, when temperature is below 873 K, NH₃ conversion on $\text{Ni}_{1.26}(\text{Al}_0.3\text{O}_n)$ is higher than that obtained on $\text{Ni}_{0.12}(\text{Mg}_{1.09}\text{Al}_0.3\text{O}_n)$. At 893 K, the NH₃ conversions over $\text{Ni}_{0.6}(\text{Mg}_x\text{Al}_y\text{O}_n)$ ($x/y=1-3$) attain the thermodynamic equilibrium value (99.92%) and are notably higher than that derived over $\text{Ni}_{1.26}(\text{Al}_0.3\text{O}_n)$. The observations suggest that increase in Ni content alone cannot achieve even higher activity, certain amount of Mg in $\text{Ni}_x(\text{Mg}_y\text{Al}_z\text{O}_n)$ is essential to enhance catalyst performance.

The effect of Mg/Al molar ratio on the catalytic activity of $\text{Ni}_{0.6}(\text{Mg}_y\text{Al}_z\text{O}_n)$ in NH₃ decomposition was illustrated in Fig. 1b. Ru/Al₂O₃ and Ru-K/Al₂O₃ were also tested for comparison. In the 723–873 K range, the NH₃ conversion over $\text{Ni}_{0.6}(\text{Mg}_y\text{Al}_z\text{O}_n)$ showed

Table 2

A comparison of ammonia decomposition activity over a number of catalyst systems at 873 K.

Catalyst	GHSV (ml h ⁻¹ g _{cat} ⁻¹)	Conv. (%)	H ₂ formation rate (mmol min ⁻¹ g _{cat} ⁻¹)	Ref.
K-Ni/MCM-41(TIE)	30,000	73.2	24.5	[32]
Nano-Ni+0.1La@SiO ₂	30,000	96.2	32.2	[33]
Ni _{1.20} Ce _{0.10} Al	30,000	99.0 ± 1.0	33.2 ± 0.3	[34]
Ni/La ₂ O ₃ (citric acid complex method)	6000	95.0 ± 1.0	6.4 ± 0.1	[35]
15%-Ni/MRM-600	30,000	55.0 ± 1.0	18.4 ± 0.3	[36]
Ni _{1.26} (Al _{0.3} O _n)	30,000	80.1	26.82	This study
Ni _{0.6} (Mg _{0.29} Al _{0.57} O _n)	30,000	99.3	33.3	This study

Among the Ru-based catalysts, Ru-K/CNTs [8] was found to be the most active one so far.

the following order: Ni_{0.6}(Mg_{0.29}Al_{0.57}O_n) > Ni_{0.6}(Mg_{0.43}Al_{0.44}O_n) = Ni_{0.61}(Mg_{0.6}Al_{0.3}O_n) = Ni_{0.6}(Mg_{0.64}Al_{0.23}O_n) > Ni_{0.6}(Al_{0.83}O_n), alone with the molar ratio of Mg/Al varying from 0 to 3. At 893 K, the NH₃ conversion over Ni_{0.6}(Mg_yAl_zO_n) reached the thermodynamic equilibrium value at the Mg/Al ratio being 0.5–2; while at 903 K, the NH₃ conversion over Ni_{0.6}(Mg_{0.64}Al_{0.23}O_n) reached the thermodynamic equilibrium value. Ni_{0.6}(Al_{0.83}O_n) without Mg constituent showed the lowest NH₃ conversion among the serial samples, and the thermodynamic equilibrium state was accomplished at 923 K. Both Ru/Al₂O₃ and Ru-K/Al₂O₃ showed higher activity than Ni_x(Mg_yAl_zO_n) in the 723–823 K range. At 723 K, the NH₃ conversion over Ru-K/Al₂O₃ is 41.65%, notably higher than that (17.38%) obtained on Ni_{0.6}(Mg_{0.29}Al_{0.57}O_n). Interestingly, the superiority of the Al₂O₃ supported Ru catalysts became diminishing with increasing reaction temperature: As temperature was beyond 823 K, the NH₃ conversion over Ru/Al₂O₃ was lower than that on Ni_{0.6}(Mg_{0.29}Al_{0.57}O_n). At 853 K, even over the potassium-doped Ru/Al₂O₃, the NH₃ conversion (92.5%) became lower than that (96.3%) obtained on Ni_{0.6}(Mg_{0.29}Al_{0.57}O_n). The observations suggest that at moderate temperatures the current Ni_x(Mg_yAl_zO_n) catalysts with a certain Ni, Mg, and Al stoichiometry exhibit better activity in NH₃ decomposition even compared with the Ru/Al₂O₃ and Ru-K/Al₂O₃ catalysts. It is worth noting that the Ru-K/CNTs catalyst is still more active than Ru/Al₂O₃ and Ru-K/Al₂O₃ for NH₃ decomposition [8]. A comparison of ammonia decomposition over a number of the Ni-based systems at 873 K is summarized in Table 2. Clearly, Ni_{0.6}(Mg_{0.29}Al_{0.57}O_n) showed the very best performance among the typical examples reported in recent years [32–36]. Moreover, the presence of certain Mg sites enhanced catalyst performance [Table 1, Ni_{0.6}(Mg_{0.29}Al_{0.57}O_n) vs. Ni_{1.26}(Al_{0.3}O_n)]. The current NiMgAl-LDH derived Ni_x(Mg_yAl_zO_n) catalysts comprise abundant Mg and Al constituents, and are even free of rare earth elements. This is significantly cost effective when considering commercial practice. Moreover, our Ni_{0.61}(Mg_{0.6}Al_{0.3}O_n) catalyst showed excellent stability in the target reaction: it was very durable for a time on stream of nearly 150 h, operated alternatively at 823 K and 893 K (Fig. 2), which is comparable to the core-shell structured Ni catalyst previously fabricated by us for the same reaction [33]. Such a feature of the Ni_x(Mg_yAl_zO_n) catalyst is important for a potential application in a large scale. For the carbon-containing catalyst, it is challenging to maintain long term durability due to the inevitable side reaction such as the methanation of carbon material in a hydrogen rich atmosphere such as the one of ammonia decomposition.

3.2. Characterizations

3.2.1. XRD

The XRD patterns of the uncalcined LDH precursors are shown in Fig. 3a. All of the samples show the diffraction peaks at 2θ = 11°, 22°, 34°, 39°, 60°, and 62°, corresponding to the (003), (006), (009), (015), (110), and (113) reflections of a typical LDH structure. Only a single crystal phase can be identified, suggesting an isomorphic replacement of Mg²⁺ by Ni²⁺ in the hydroxide layers. This

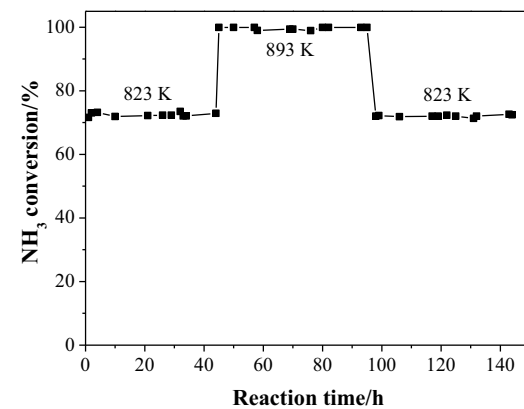
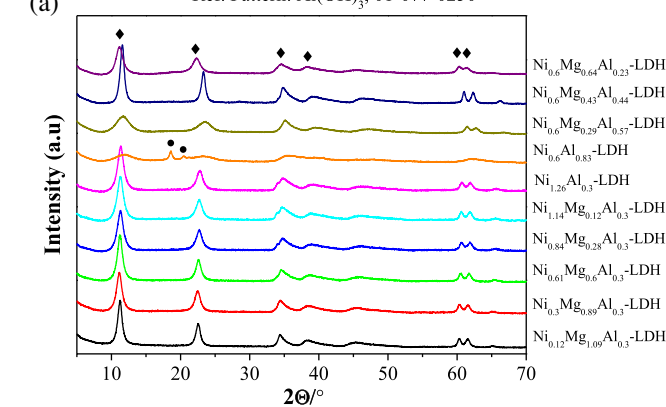


Fig. 2. NH₃ conversion as a function of reaction time over Ni_{0.61}(Mg_{0.6}Al_{0.3}O_n). GHSV_{NH₃} = 30,000 ml h⁻¹ g_{cat}⁻¹.

- ◆ Ref. Pattern: Hydrotalcite-like compound, 00-014-0191
- Ref. Pattern: Al(OH)₃, 01-077-0250



- * Ref. Pattern: MgNiO₂, 00-024-0712
- Ref. Pattern: NiO, 03-065-6920
- ◆ Ref. Pattern: MgO, 00-001-1235

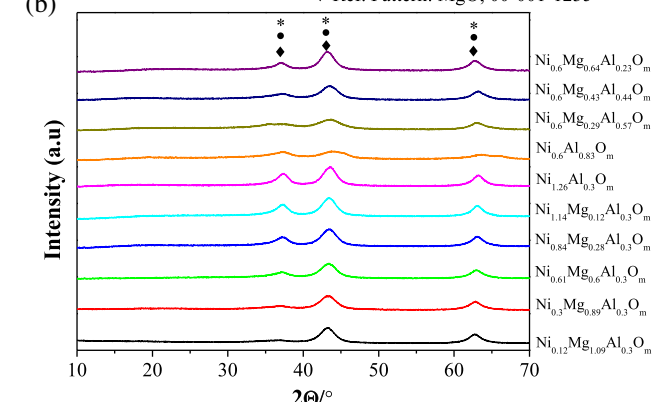


Fig. 3. XRD patterns of (a) Ni_xMg_yAl_z-LDH, and (b) Ni_xMg_yAl_zO_m.

ensures a homogeneous inter-dispersion of all constituents in the calcined forms. Brindley et al. reported that the Ni, Al-containing LDH can be synthesized with the $\text{Al}^{3+}/(\text{Ni}^{2+} + \text{Al}^{3+})$ ratio being in the 0.2–0.33 range [37]. In this study, a LDH precursor with the ratio of $\text{Al}^{3+}/(\text{Ni}^{2+} + \text{Al}^{3+}) = 0.6$ was synthesized. There is excessive Al^{3+} in this sample, and therefore the XRD pattern shows additional peaks at $2\theta = 18^\circ$ and 20° , attributable to the (001) and (020) reflections of the free $\text{Al}(\text{OH})_3$ species. The lattice parameters c and a of the LDH structure, related to the average interlayer and cation-cation distances, can be calculated by employing the equations $c = 3d_{003}$ and $a = 2d_{110}$, respectively. The value of parameter a is related to the ionic radii of the layer cations, while the value of parameter c is determined by the nature and orientation of the interlayer anions. With gradual substitution of Mg^{2+} (0.072 nm) by Ni^{2+} (0.069 nm), the parameter c nearly unchanged while the parameter a decreased accompanying with the shorter cation-cation distance. On the other hand, upon gradual replacing Al^{3+} (0.0535 nm) with Mg^{2+} (0.072 nm), both parameters a and c increased because of the extended cation-cation distance as well as the two looser hydroxide layers.

Fig. 3b illustrates the XRD patterns of the calcined samples, $\text{Ni}_x\text{Mg}_y\text{Al}_z\text{O}_m$. The characteristic reflections indexed to the LDH structure completely disappeared. In terms of the reflection peaks as well as the constitution of samples, there might exist MgO , NiO , and/or $\text{Ni}-\text{Mg}-(\text{Al})-\text{O}$ solid solution in the calcined samples. Actually the exact identification of phase structure (MgO , NiO , and/or $\text{Ni}-\text{Mg}-(\text{Al})-\text{O}$) is rather difficult. Moreover, there is considerable structural rearrangement of the mixed oxide upon the following high temperature H_2 -reduction. Therefore, we did not calculate the average crystallite size of the oxide precursor from the XRD patterns. Instead, we made statistical analysis of metallic Ni particles (they are active component for the reaction), and plotted the average Ni^0 particle size with the Ni/Mg or Mg/Al ratio (Fig. S1, S2, see the Discussion in the TEM section).

3.2.2. H_2 -TPR

H_2 -TPR was carried out to investigate the interaction between the NiO component and the matrix. **Fig. 4** shows the H_2 -TPR profiles of $\text{Ni}_x\text{Mg}_y\text{Al}_z\text{O}_m$. All the samples show only one reduction peak, indicating structurally homogeneous Ni^{2+} species inherited from the LDH structure. The gradual substitution of Ni^{2+} by Mg^{2+} in $\text{Ni}_x\text{Mg}_y\text{Al}_z\text{O}_m$ causes the reduction peak obviously shifting to the higher temperature end (from 802 to 1103 K), along with increasing interaction between Mg and Ni cations. As a matter of fact, the gradually increased reduction temperature could be attributed to the formation of $\text{Ni}-\text{Mg}-(\text{Al})-\text{O}$ solid solution. On the other hand, the variation in Mg/Al molar ratio gives rise to insignificant change in the reduction temperature. With increasing Mg/Al ratio from 0.5 to 3, the reduction peak gradually shifts from 960 to 900 K. $\text{Ni}_{0.6}\text{Al}_{0.83}\text{O}_m$ shows slightly lower reduction temperature than $\text{Ni}_{0.6}\text{Mg}_{0.64}\text{Al}_{0.23}\text{O}_m$, which could be explained by the existence of free $\text{Al}(\text{OH})_3$ species that destroys the structural integrity of the LDH precursor to some extent. The observation suggests that the interaction between Ni and Al cations is likely stronger than that between Ni and Mg cations. Takehira and co-workers [38] reported a spc-Ni/MgAl catalyst showing the reduction peak temperature beyond 1100 K, ascribed to the formation of NiAl_2O_4 spinel on the catalyst surface. It is difficult to distinguish the NiAl_2O_4 spinel phase in the XRD patterns of this study, however, since the reduction temperature of Ni^{2+} generally exceeds 900 K, it is reasonable to assume that some spinel-like NiAl_aO_b with low crystallinity may exist in $\text{Ni}_x\text{Mg}_y\text{Al}_z\text{O}_m$.

The reduction temperature of Ni^{2+} is mainly influenced by the Ni content of $\text{Ni}_x\text{Mg}_y\text{Al}_z\text{O}_m$, and also related to the kind of lattice oxygen species in the samples. The formation of $\text{Ni}-\text{Mg}-(\text{Al})-\text{O}$ solid solution can increase the reduction temperature of the cor-

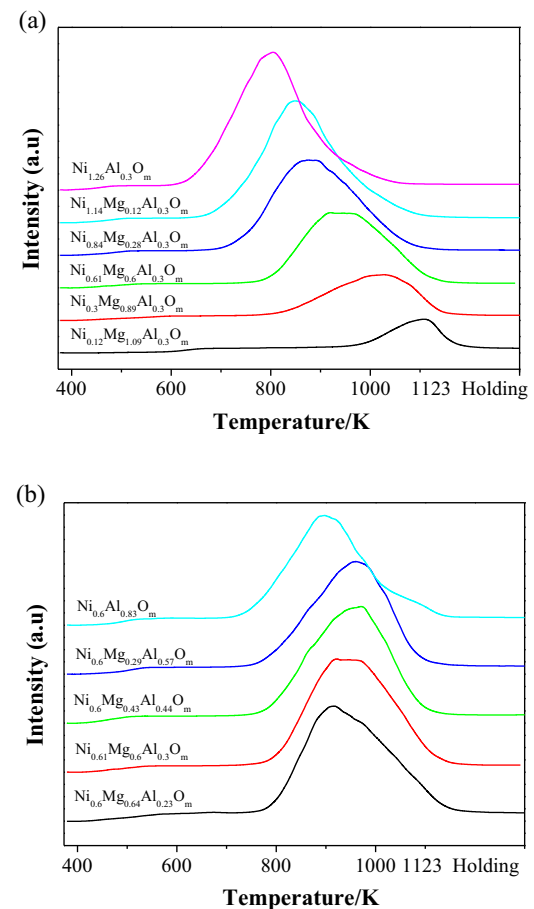


Fig. 4. H_2 -TPR profiles of (a) $\text{Ni}_x\text{Mg}_y\text{Al}_z\text{O}_m$, and (b) $\text{Ni}_{0.6}\text{Mg}_y\text{Al}_z\text{O}_m$.

responding Ni^{2+} species. It is deduced that the $\text{Ni}-\text{Mg}-(\text{Al})-\text{O}$ solid solution, though likely non-stoichiometric, could exist in the precursor. The $\text{Ni}-\text{OH}$ and $\text{Mg}/\text{Al}-\text{OH}$ could condense together in the edges to form the $\text{Ni}-\text{O}-\text{Mg}/\text{Al}$ during the calcination step. The Ni^{2+} cations with the saturated lattice oxygen have the lowest $\text{Ni}-\text{O}$ binding energy and therefore can be the most easily reducible. With gradual replacement of Ni by Mg/Al, the lattice oxygen becomes more structurally stable and more difficultly removable.

3.2.3. TEM

TEM technique was used to check the overall morphology of the reduced $\text{Ni}_x(\text{Mg}_y\text{Al}_z\text{O}_n)$ samples, particularly the state of metallic Ni particles. As shown in **Fig. 5**, the Ni nanoparticles are essentially uniformly distributed throughout the matrix. With increasing Ni/Mg molar ratio in $\text{Ni}_x(\text{Mg}_y\text{Al}_z\text{O}_n)$, the density and the particle size of Ni grains increase accordingly (**Fig. 5a-f**). When the Ni/Mg molar ratio exceeds 3, aggregation of Ni particles appears noticeable (**Fig. 5d-f**). The correlation between the average Ni particle size and the Ni/Mg molar ratio has been clearly indicated in Fig. S1 (Supplementary material). On the other hand, increase in Mg/Al molar ratio from 0.5 to 3 results in a small increment in Ni particle size (**Fig. 5c, h-j**, and **Fig. S2**). Note that, different from $\text{Ni}_{1.26}(\text{Al}_0.3\text{O}_n)$, $\text{Ni}_{0.6}(\text{Al}_0.83\text{O}_n)$ shows the Ni particles similar to those in $\text{Ni}_{0.6}(\text{Mg}_{0.64}\text{Al}_{0.23}\text{O}_n)$. This suggests that the ratio of $\text{Ni}/(\text{Mg} + \text{Al})$ mainly determine the Ni particle size as well as the particle distribution. The H_2 -TPR results revealed that the samples which were reduced at higher temperatures would generate smaller Ni^0 particles. The enhanced metal-oxide matrix interaction effectively hinders the migration and aggregation of Ni nanoparticles upon reduction. The catalyst eventually used for the reaction

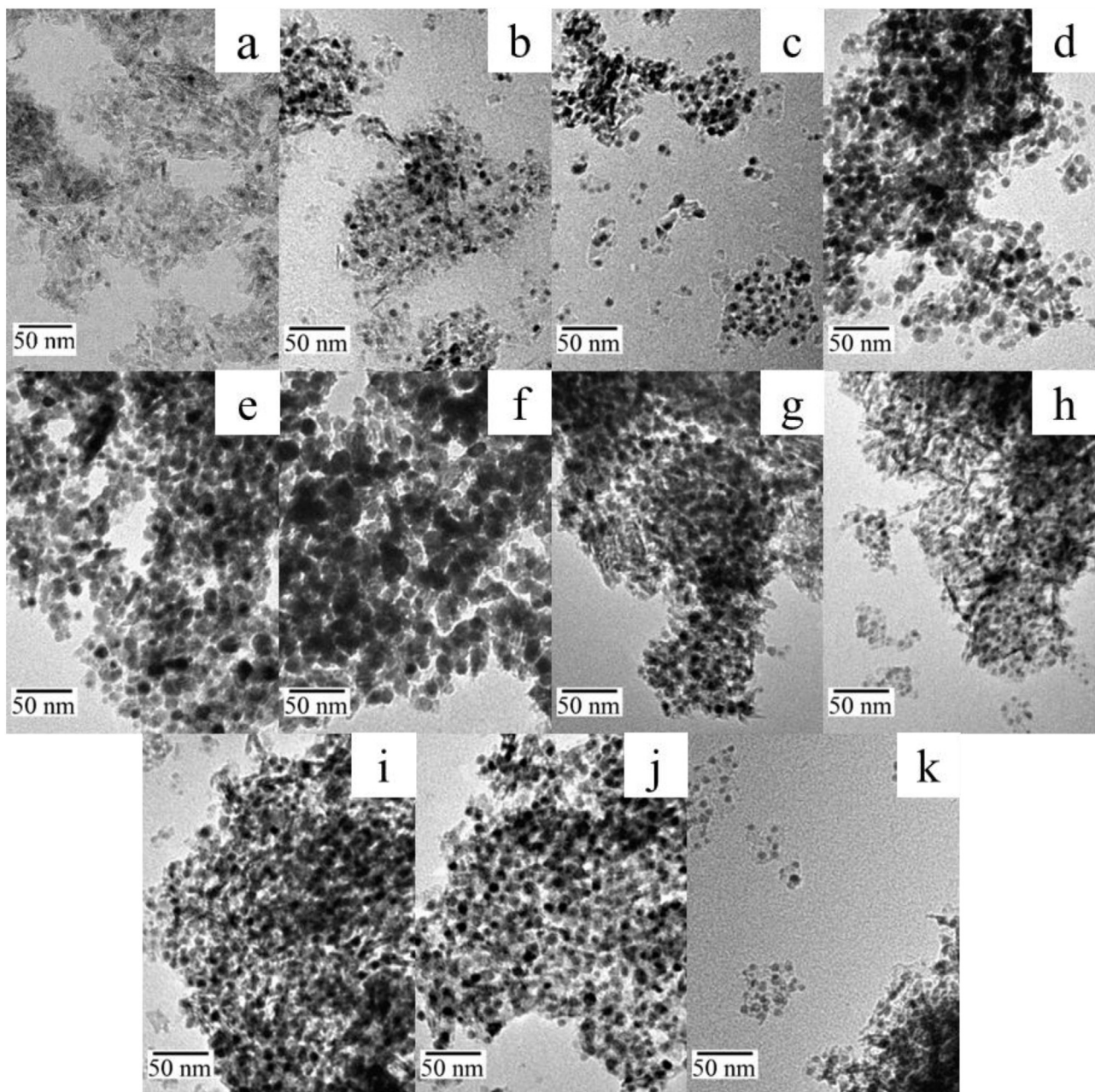


Fig. 5. TEM images of (a) $\text{Ni}_{0.12}(\text{Mg}_{1.09}\text{Al}_{0.3}\text{O}_n)$, (b) $\text{Ni}_{0.3}(\text{Mg}_{0.89}\text{Al}_{0.3}\text{O}_n)$, (c) $\text{Ni}_{0.61}(\text{Mg}_{0.6}\text{Al}_{0.3}\text{O}_n)$, (d) $\text{Ni}_{0.84}(\text{Mg}_{0.28}\text{Al}_{0.3}\text{O}_n)$, (e) $\text{Ni}_{1.14}(\text{Mg}_{0.12}\text{Al}_{0.3}\text{O}_n)$, (f) $\text{Ni}_{1.26}(\text{Al}_{0.3}\text{O}_n)$, (g) $\text{Ni}_{0.6}(\text{Al}_{0.83}\text{O}_n)$, (h) $\text{Ni}_{0.6}(\text{Mg}_{0.29}\text{Al}_{0.57}\text{O}_n)$, (i) $\text{Ni}_{0.6}(\text{Mg}_{0.43}\text{Al}_{0.44}\text{O}_n)$, (j) $\text{Ni}_{0.6}(\text{Mg}_{0.64}\text{Al}_{0.23}\text{O}_n)$, and (k) $\text{Ni}_{0.61}(\text{Mg}_{0.6}\text{Al}_{0.3}\text{O}_n)$ after reaction of 144 h.

experienced the treatments of calcination and reduction, involving the removal of H_2O , CO_3^{2-} , $-\text{OH}$, and O^{2-} species from the LDH structured precursor, and accompanying considerable texture variation in the samples [39–41]. The metal nanoparticles that are well isolated and immobilized in the porous matrix can be more thermally stable yet easily accessible to the reactant. Fig. 5k shows the TEM image of $\text{Ni}_{0.61}(\text{Mg}_{0.6}\text{Al}_{0.3}\text{O}_n)$ after a reaction of 144 h. It is clearly evident that the Ni particle size is almost identical to that of the freshly reduced sample (Fig. 5c). The excellent structure stability is in accordance with its unique structural feature aforementioned.

3.2.4. Turnover frequency (TOF)

The activity comparison based on the unit mass of catalyst is insufficient because the exposed Ni surface area is different among serial samples. And because of this, the activity comparison was also

made based on the exposed area of metal Ni (or the Ni dispersion) which was determined by pulse H_2 -chemisorption. In the latter case, the activity was normalized to each surface Ni atom in various samples (i.e. on the basis of TOF values), so that the effect of variation in surface area of Ni on activity has been eliminated. Hereby, the TOF value of each catalyst was calculated to compare the catalytic activity: Normalizing the observed reaction rate (mole H_2 formed per gram of catalyst per second) to the number of exposed Ni surface atoms per gram of catalyst (derived from the H_2 pulse chemisorption experiments assuming adsorption of one H atom over per surface Ni atom).

It is worth noting that the conditions for the pulse H_2 -adsorption and the exposed Ni surface measurements of this study have been widely applied in the previous reports [42–46]. In order to minimize the spillover effect on the determination of Ni surface, the pulse adsorption temperature and pressure were set to be 323 K

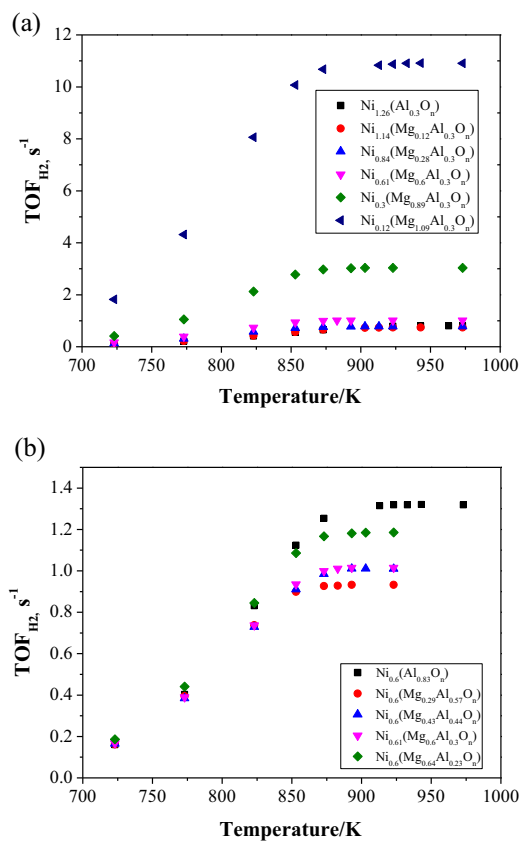


Fig. 6. Comparison of TOF values of H₂ formation over (a) Ni_x(Mg_yAl_{0.3}O_n) and (b) Ni_{0.6}(Mg_yAl₂O_n) at different temperatures.

and atmospheric, as mostly did in literature reports. Therefore, it is believed that the spillover of hydrogen is insignificant under the conditions of pulse H₂-adsorption. Even if the spillover of hydrogen cannot be completely excluded, the activity order over the sample series is still retained, because the exposed Ni surface will be overestimated and thus the TOF value underestimated when the spillover of hydrogen exists, especially for the smaller Ni particles. That is to say, the catalyst activity with a higher TOF value in this study could be somewhat underestimated if the spillover effect exists at the pulse H₂ adsorption conditions. Nevertheless, the activity order of the sample series based on the TOF values keeps unchanged regardless of possible spillover of hydrogen if any. On the other hand, Fang et al. [47] and Salam et al. [48] recently reported that hydrogen could present in the bulk phase of the mixed oxide derived from hydrotalcites. Hydrogen diffusion into oxide bulk phase should be kinetically unfavorable at the mild conditions used for pulse H₂-adsorption, while it could become noticeable only at high reaction temperatures.

As shown in Fig. 6, the TOF values calculated for all of catalysts first increase and then level off with increasing reaction temperature, showing similar trends to the NH₃ conversions. There is a clearer trend indicated between the TOF value and the Mg/Ni ratio (Fig. S3). As the Mg/Ni ratio changes from 0 to 1, the TOF value increases by a factor <1 within the temperature range studied. As the Mg/Ni ratio varies from 1 to 3, the TOF value increases dramatically by a factor of 3 at 853 K. Ni_{0.12}(Mg_{1.09}Al_{0.3}O_n)(Mg/Ni = 9) provides the highest TOF value: nearly three times greater than that achieved over Ni_{0.3}(Mg_{0.89}Al_{0.3}O_n). The highest NH₃ conversion rate over Ni_{0.61}(Mg_{0.6}Al_{0.3}O_n) is attributable to the abundant yet efficient sites on the catalyst surface. It appears that a catalyst with a relatively lower Ni content shows a higher reaction rate on the basis of turnover frequency (Table 3). The exposed sur-

Table 3
The exposed Ni atoms and the TOF values of H₂ formation over various samples.

Sample	Exposed Ni atoms (mmol g _{cat} ⁻¹)	TOF _{H₂} (s ⁻¹ , 823 K)
Ni _{0.12} (Mg _{1.09} Al _{0.3} O _n)	40.0	8.1
Ni _{0.3} (Mg _{0.89} Al _{0.3} O _n)	183.9	2.1
Ni _{0.61} (Mg _{0.6} Al _{0.3} O _n)	549.4	0.7
Ni _{0.84} (Mg _{0.28} Al _{0.3} O _n)	712.9	0.6
Ni _{1.14} (Mg _{0.12} Al _{0.3} O _n)	751.1	0.4
Ni _{1.26} (Al _{0.3} O _n)	693.2	0.4
Ni _{0.6} (Al _{0.83} O _n)	422.4	0.8
Ni _{0.6} (Mg _{0.29} Al _{0.57} O _n)	597.6	0.7
Ni _{0.6} (Mg _{0.43} Al _{0.44} O _n)	551.6	0.7
Ni _{0.6} (Mg _{0.64} Al _{0.23} O _n)	470.5	0.8

Table 4
CO₂ uptake over various samples.

Sample	Amount of CO ₂ desorbed (mmol g _{cat} ⁻¹)
Ni _{0.12} (Mg _{1.09} Al _{0.3} O _n)	3.54
Ni _{0.3} (Mg _{0.89} Al _{0.3} O _n)	3.42
Ni _{0.61} (Mg _{0.6} Al _{0.3} O _n)	3.27
Ni _{0.84} (Mg _{0.28} Al _{0.3} O _n)	2.99
Ni _{1.14} (Mg _{0.12} Al _{0.3} O _n)	2.55
Ni _{1.26} (Al _{0.3} O _n)	1.79
Ni _{0.6} (Al _{0.83} O _n)	3.66
Ni _{0.6} (Mg _{0.29} Al _{0.57} O _n)	2.66
Ni _{0.6} (Mg _{0.43} Al _{0.44} O _n)	4.07
Ni _{0.6} (Mg _{0.64} Al _{0.23} O _n)	3.34

face Ni atoms decrease smoothly with reducing Ni content. Note that Ni_{0.12}(Mg_{1.09}Al_{0.3}O_n) has the lowest Ni content meanwhile its Ni surface exposure becomes extraordinarily low, suggesting a close contact between the Ni nanoparticles and the oxide matrix. It is understandable, because Ni_{0.12}(Mg_{1.09}Al_{0.3}O_n) has the smallest Ni particle size (Fig. 5a and Fig. S1), and the closely contacted neighboring Mg sites around the very fine Ni particles may have a stronger synergistic effect on the Ni sites for the catalytic process. The promotion effect of alkali/alkaline earth metal elements on NH₃ decomposition has been recognized in the previous investigations [3,4,8]. Yin et al. [3,4] and Aika et al. [49] pointed out that the surface basicity of catalyst favored both NH₃ decomposition and synthesis reactions. The presence of alkali or alkaline earth metal element would enhance the electron density of active metal such as Ru, which in turn facilitated desorption of surface nitrogen atoms. The current study further illustrated that an interaction between the active metal of Ni and the Mg-containing species could favor adsorption/activation of NH₃, resulting in activity enhancement. It appears that the appropriate synergic effect between Ni and basic sites involves the electron-donating of Mg sites to Ni, the control of Mg site density and Ni particle size, as well as their effective junction, yielding an optimal promotion on activity in line with the change of Ni/Mg ratio in sample series.

Fig. 6b shows the comparison in the TOF values of H₂ formation over Ni_{0.6}(Mg_yAl₂O_n) at different temperatures. The effect of the Mg/Al ratio on the corresponding TOF values was found to be less significant than that of the Mg/Ni ratio (Fig. S4). The TOF value slightly increases with increasing Mg/Al ratio from 0.5 to 3 under the same reaction conditions. Below 853 K, the TOF value of Ni_{0.6}(Al_{0.83}O_n) is somewhat lower than that of Ni_{0.6}(Mg_{0.64}Al_{0.23}O_n); while beyond 853 K, the reverse situation can be observed. The phenomenon is somehow unexpected, and to better understand this observation, further characterizations including CO₂-TPD and H₂-TPD have been carried out and the results are presented below (Table 4).

3.2.5. CO₂-TPD

There are a number of researches showing the promotion effect of the basic sites on NH₃ decomposition over the Ru and Ni metal

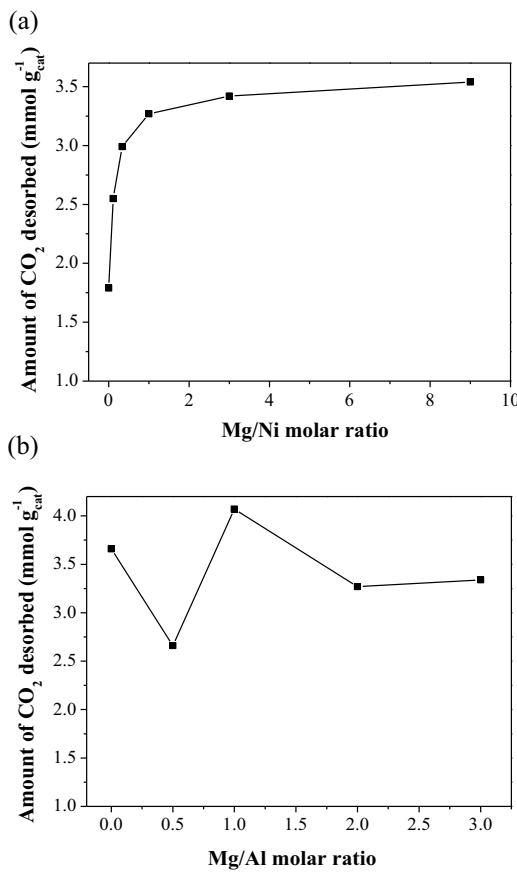


Fig. 7. Amount of CO_2 desorbed changes with (a) Mg/Ni and (b) Mg/Al ratios.

catalysts [8,35,50–52]. Therefore, the surface basicity of catalyst is crucial to influence the corresponding catalytic behavior. Herein, CO_2 was employed as a probe molecule to compare the surface basicity of $\text{Ni}_x(\text{Mg}_y\text{Al}_z\text{O}_n)$ and the results are shown in Fig. 7. It is observed that the density of basic sites (relevant to the desorption peak area) is highly dependent on the $\text{Ni}/(\text{Mg} + \text{Al})$ ratio. The quantitative analysis of the CO_2 -TPD profiles has been performed and the results are summarized in Table 4. For $\text{Ni}_x(\text{Mg}_y\text{Al}_0.3\text{O}_n)$ with various Mg/Ni molar ratios, the density of basic sites increases rapidly with increasing Mg/Al ratio up to 1.0, then changes slowly with further increasing Mg/Ni ratio (Fig. 7a). However, for $\text{Ni}_{0.6}(\text{Mg}_y\text{Al}_z\text{O}_n)$ with different Mg/Al molar ratios, the density of basic sites varies rather irregularly with increasing Mg/Al ratio (Fig. 7b). The observed difference is thought to be associated with the related structural change. The Ni^{2+} and Mg^{2+} cations are the same in valence state but different in ionic radius. As the content of Mg^{2+} changes with respect to that of Ni^{2+} , the resulting cation-cation distance in the mixed metal hydroxide layers is primarily affected. When the content of Mg^{2+} varies with respect to that of Al^{3+} , both the electron charge and the cation-cation distance of layers will be affected. The amount and orientation of interlayer anions should adjust accordingly to balance the charge of the layers, resulting in the reformation of whole structure.

We plotted the TOF value with the Mg/Ni ratio at typical reaction temperatures, and found that the former changes monotonously with the latter (Fig. S3). However, the TOF value changes quite differently with the Mg/Al ratio (Fig. S4). As mentioned before, the density of basic sites also varies rather irregularly with the Mg/Al ratio (Fig. 7b). Therefore, it seems to be difficult to establish a correlation between the TOF value and the density of surface basic sites by changing the Mg/Al ratio. The results suggest that surface basicity of catalyst may be one of the factors accounting for the observed

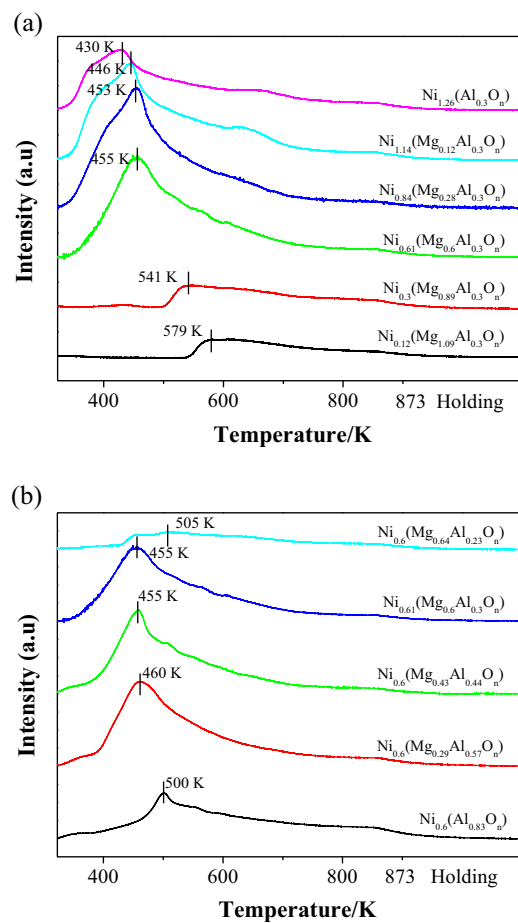


Fig. 8. H_2 -TPD profiles obtained on (a) $\text{Ni}_x(\text{Mg}_y\text{Al}_0.3\text{O}_n)$ and (b) $\text{Ni}_{0.6}(\text{Mg}_y\text{Al}_z\text{O}_n)$.

catalyst performance; and there could be other important factor behind responsible for the different catalytic behavior.

3.2.6. H_2 -TPD

The decomposition of NH_3 generates N_2 and H_2 . It is known that the chemisorption of N_2 on Ni is weak, whereas the chemisorption of H_2 on Ni can be rather strong. This implies that desorption of H_2 from Ni surface could play an important role in the catalytic process. In order to figure out the impact of this aspect, the H_2 -TPD experiments were conducted over the serial samples. As shown in Fig. 8, there are two situations observed for the H_2 -TPD profiles. The peak essentially shifts to the higher temperature end (from 430 K to 579 K) over the sample series with increasing Mg/Ni ratio (Fig. 8a). By varying the Mg/Ni molar ratio from 0 to 1, there is one large desorption peak centered around 450 K with noticeable tailing in each TPD profile, suggesting the presence of some high-temperature desorbed species. With further increasing Mg/Ni ratio to 3, there are two peaks in the TPD profile, the small one at about 450 K and the large one at 541 K. Only one broad peak at 579 K can be observed as the Mg/Ni ratio reaches 9. On the other hand, peak shift becomes irregular and insignificant over the sample series with increasing Mg/Al ratio (Fig. 8b).

Making a comparison in the results of thermal desorption investigations, one can observe that the sequence of desorption peak temperature just follows the order of TOF value. The higher the temperature of H_2 -desorption peak is, the higher the corresponding TOF value will be. Similar phenomenon has been previously observed by Yin and co-workers on the Ru-based catalysts [53]. There could be certain inherent correlation between the behavior of surface H species and the related TOF values. It is worth

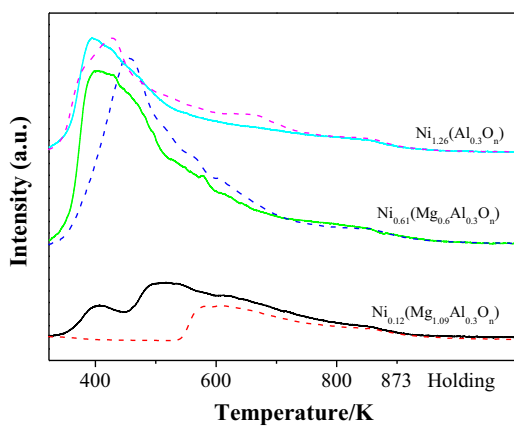


Fig. 9. Comparison of H₂-TPD profiles corresponding to pre-adsorption of H₂ at 373 K (solid line) and 323 K (dashed line).

noting that Ni_{0.12}(Mg_{1.09}Al_{0.3}O_n) showing the highest TOF value only has one desorption peak at 579 K, which is obviously different from the situations observed on the other samples. The adsorption/desorption behavior of surface hydrogen species would have a curial effect on the availability of surface active site. The shift of desorption peak to the high-temperature end was attributed to the spillover effect of surface hydrogen species suggested by different researchers [54–57]. According to the H₂-TPD study, it is reasonable to infer that there is a spillover phenomenon for surface hydrogen species involving in the surface reaction of NH₃ decomposition on the current catalysts. And the extent of spillover effect seems to be directly associated with the Mg/Ni ratios (i.e., the Ni local structure environment and the Ni-Mg interaction). To sustain this speculation, additional H₂-TPD experiments were conducted in which the pre-adsorption of H₂ was operated at a higher temperature of 373 K. The TPD profiles obtained from two cases were then compared each other. Over Ni_{0.12}(Mg_{1.09}Al_{0.3}O_n), one can clearly find that desorption of surface hydrogen is enhanced by high-temperature pre-adsorption. Such an observation also verified the occurrence of hydrogen spillover effect [57–60]. When the hydrogen adsorption was operated at 373 K, additional desorption peak appeared at the lower temperature end over Ni_{0.12}(Mg_{1.09}Al_{0.3}O_n), attributable to the enhanced hydrogen spillover effect resulted from the higher temperature pre-adsorption of hydrogen. The strong spillover effect favors the migration of surface H species and leaves the unoccupied Ni sites for adsorption of more hydrogen molecules. The overall amount of adsorbed/desorbed hydrogen is thus increased, accounting for the appearance of the low-temperature desorption peak. As the hydrogen adsorption was operated at a low temperature (323 K), the low-temperature desorption peak was absent. It does not mean there is a variation in the total number of surface Ni sites. In fact, because of the spillover effect, the adsorbed hydrogen could easily migrate along the surface during the temperature programmed course, and would desorb at higher temperatures. Moreover, the desorption profiles corresponding to the hydrogen adsorption at 373 K over Ni_{0.61}(Mg_{0.6}Al_{0.3}O_n) and Ni_{1.26}(Al_{0.3}O_n) also showed peak shift toward low temperature end as well as peak area increment, suggesting an enhanced adsorption of hydrogen. According to the examples shown in Fig. 9, the spillover effect is exactly strengthened by the Mg constituent of certain amount in the samples. Over Ni_{0.61}(Mg_{0.6}Al_{0.3}O_n), the spillover effect becomes less significant, whereas over Ni_{1.26}(Al_{0.3}O_n) without any Mg, the spillover effect is the least obvious. This is understandable, because there are the finest Ni grains and the strongest Ni-oxide matrix contact and interaction in Ni_{0.12}(Mg_{1.09}Al_{0.3}O_n), leading to the most significant spillover effect (Fig. 9).

As the hydrogen spillover effect is enhanced, more surface hydrogen species migrates from the metal surface to the metal-oxide boundary and further to the oxide matrix surface. They are likewise stabilized and desorb at higher temperatures, accounting for the observations made. Bear in mind that the activation energy for the diffusion of surface hydrogen is notably lower than that for the direct desorption, therefore, a catalyst that has a strong potential for the spillover effect of surface hydrogen can more quickly recover the active sites for the following reactant molecules, undergoing a more efficient surface reaction as a result. If there is a weak hydrogen spillover effect on the catalyst surface, the H species from the dissociation of the N–H bond in NH₃ could stick on the active Ni sites, blocking the follow-up NH₃ molecules for adsorption/activation.

The H₂-TPR results indicate that the reduction temperature shifts toward higher temperature end with decreasing Ni content in the sample series. A concern about the reducibility of Ni²⁺ in low content could be raised, which might have an effect on hydrogen spillover. Note that, however, the conditions employed for continuous reduction of mixed oxide (at a constant temperature of 973 K in a 25% H₂/Ar flow of 100 ml/min for 2 h) is actually severer than that employed for H₂ temperature programmed reduction (from 373 K to 1123 K at a ramp of 10 K/min in a 10% H₂/Ar flow of 40 ml/min). In other words, even the sample of the lowest Ni content, Ni_{0.12}Mg_{1.09}Al_{0.3}O_m, can be sufficiently reduced in the applied H₂ pre-reduction. To verify this, Ni_{0.12}Mg_{1.09}Al_{0.3}O_m was first subjected to a continuous reduction at 973 K in a 25% H₂/Ar flow of 100 ml/min for 2 h and then followed by a typical H₂-TPR procedure of the current study. The H₂-TPR profile reveals that the Ni cations, even in the lowest content, are essentially reduced by the employed H₂ pre-reduction.

4. Concluding remarks

The NiMgAl-LDH structures with different stoichiometric ratio of Ni/Mg and Mg/Al were synthesized and used as the catalyst precursors for NH₃ decomposition. The results verified high catalytic efficiency as well as excellent durability of the derived Ni-based catalysts. This kind of Ni catalyst is attractive for large-scale operation owing to the features of cost effective, easy fabrication, and good stability. The characterizations detailed the information about the Ni particles size and distribution, the Ni-oxide matrix interaction, the surface basicity, and the adsorption/desorption behavior of hydrogen changing with the stoichiometry of Ni, Mg, and Al in the samples. The superior catalyst performance is interpreted in terms of the unique structure of Ni species and the Mg-Ni synergism. Particularly, the spillover effect of surface hydrogen was recognized to accelerate the reaction cycles over the active Ni sites. The homogeneous inter-dispersion of metal-oxide constituents ensures good isolation of Ni particles and outstanding catalyst stability as a result.

Acknowledgements

We greatly appreciated the financial support from NSFC (21173118, 21373110), and MSTA (2013AA031703). Q. Su and W. J. Ji are especially grateful to Professor Y. M. Wang for his kind assistance in this work.

Appendix A. Supplementary data

Supplementary data associated with this article can be found, in the online version, at <http://dx.doi.org/10.1016/j.apcatb.2016.08.051>.

References

- [1] T.V. Choudhary, D.W. Goodman, *Catal. Lett.* 59 (1999) 93–94.
- [2] T.V. Choudhary, C. Sivadarayana, D.W. Goodman, *Catal. Lett.* 72 (2001) 197–201.
- [3] S.F. Yin, B.Q. Xu, X.P. Zhou, C.T. Au, *Appl. Catal. A: Gen.* 277 (2004) 1–9.
- [4] E. García-Bordejé, S. Armenise, L. Roldán, *Catal. Rev.* 56 (2014) 220–237.
- [5] M.V. Gil, J. Fermoso, C. Pevida, D. Chen, F. Rubiera, *Appl. Catal. B: Environ.* 184 (2016) 64–76.
- [6] R. van Santen, M. Neurock, G. Ertl, H. Knözinger, J. Weitkamp (Eds.), *Handbook of Heterogeneous Catalysis*, vol. 5, Wiley-VCH Verlag GmbH & Co. KGaA Weinheim, 1997.
- [7] A. Boisen, S. Dahl, J.K. Nørskov, C.H. Christensen, *J. Catal.* 230 (2005) 309–312.
- [8] S.F. Yin, Q.H. Zhang, B.Q. Xu, W.X. Zhu, C.F. Ng, C.T. Au, *J. Catal.* 224 (2004) 384–396.
- [9] Y.X. Li, L.H. Yao, Y.Y. Song, S.Q. Liu, J. Zhao, W.J. Ji, C.T. Au, *Chem. Commun.* 46 (2010) 5298–5299.
- [10] L.H. Yao, Y.X. Li, J. Zhao, W.J. Ji, C.T. Au, *Catal. Today* 158 (2010) 401–410.
- [11] J. Zhang, H. Xu, X. Jin, Q. Ge, W. Li, *Appl. Catal. A: Gen.* 290 (2005) 87–96.
- [12] J. Zhang, H. Xu, W. Li, *Appl. Catal. A: Gen.* 296 (2005) 257–267.
- [13] L.F. Zhang, M. Li, T.Z. Ren, X. Liu, Z.Y. Yuan, *Int. J. Hydrogen Energy* 40 (2015) 2648–2656.
- [14] Y. Liu, H. Wang, J. Li, Y. Lu, Q. Xue, J. Chen, *AIChE J.* 53 (2007) 1845–1849.
- [15] C. Plana, S. Armenise, A. Monzón, E. García-Bordejé, *J. Catal.* 275 (2010) 228–235.
- [16] F. Cavani, F. Trifirò, A. Vaccari, *Catal. Today* 11 (1991) 173–301.
- [17] D. Tichit, B. Coq, *CATTECH* 7 (2003) 206–217.
- [18] D.P. Debecker, E.M. Gaigneaux, G. Busca, *Chem. Eur. J.* 15 (2009) 3920–3935.
- [19] D.L. Li, M.M. Lu, K. Aragaki, M. Koike, Y. Nakagawa, K. Tomishige, *Appl. Catal. B: Environ.* 192 (2016) 171–181.
- [20] S. Zhao, K.Z. Li, S. Jiang, J.H. Li, *Appl. Catal. B: Environ.* 181 (2016) 236–248.
- [21] A.I. Tsyganok, T. Tsunoda, S. Hamakawa, K. Suzuki, K. Takehira, T. Hayakawa, *J. Catal.* 213 (2003) 191–203.
- [22] X. Yu, N. Wang, W. Chu, M. Liu, *Chem. Eng. J.* 209 (2012) 623–632.
- [23] F.M. Cabello, D. Tichit, B. Coq, A. Vaccari, N.T. Dung, *J. Catal.* 167 (1997) 142–152.
- [24] M.J. Holgado, V. Rives, M.S. San Román, *Appl. Catal. A: Gen.* 214 (2001) 219–228.
- [25] B.M. Choudary, M.L. Kantam, A. Rahman, C.V. Reddy, K.K. Rao, *Angew. Chem. Int. Ed.* 40 (2001) 763–766.
- [26] M.J. Climent, A. Corma, S. Iborra, K. Epping, A. Velty, *J. Catal.* 225 (2004) 316–326.
- [27] W.H. Fang, S. Paul, M. Capron, F. Dumeignil, L. Jalowiecki-Duhamel, *Appl. Catal. B: Environ.* 152–153 (2014) 370–382.
- [28] W.H. Fang, S. Paul, M. Capron, A.V. Biradar, S.B. Umbarkar, M.K. Dongare, F. Dumeignil, L. Jalowiecki-Duhamel, *Appl. Catal. B: Environ.* 166–167 (2015) 485–496.
- [29] A. Corma, V. Fornés, R.M. Martín-Aranda, F. Rey, *J. Catal.* 134 (1992) 58–65.
- [30] J.I. Di Cosimo, V.K. Díez, M. Xu, E. Iglesia, C.R. Pesteguía, *J. Catal.* 178 (1998) 499–510.
- [31] V.K. Díez, C.R. Pesteguía, J.I. Di Cosimo, *J. Catal.* 215 (2003) 220–233.
- [32] X.K. Li, W.J. Ji, J. Zhao, S.J. Wang, C.T. Au, *J. Catal.* 236 (2005) 181–189.
- [33] L.H. Yao, T.B. Shi, Y.X. Li, J. Zhao, W.J. Ji, C.T. Au, *Catal. Today* 164 (2011) 112–118.
- [34] W. Zheng, J. Zhang, Q. Ge, H. Xu, W. Li, *Appl. Catal. B: Environ.* 80 (2008) 98–105.
- [35] H. Miroyama, C. Saburi, T. Matsui, K. Eguchi, *Appl. Catal. A: Gen.* 443–444 (2012) 119–124.
- [36] J.L. Cao, Z.L. Yan, Q.F. Deng, Z.Y. Yuan, Y. Wang, G. Sun, X.D. Wang, B. Hari, Z.Y. Zhang, *Catal. Sci. Technol.* 4 (2014) 361–368.
- [37] G.W. Brindley, S. Kikkawa, *Am. Miner.* 64 (1979) 836–843.
- [38] K. Takehira, T. Shishido, P. Wang, T. Kosaka, K. Takaki, *J. Catal.* 221 (2004) 43–54.
- [39] M. Bellotto, B. Rebours, O. Clause, J. Lynch, D. Bazin, E. Elkaïm, *J. Phys. Chem.* 100 (1996) 8535–8542.
- [40] J. Theo Kloprogge, R.L. Frost, *Appl. Catal. A: Gen.* 184 (1999) 61–71.
- [41] L. Chmielarz, P. Kuśtrowski, A. Rafalska-Łasocha, R. Dziembaj, *Thermochim. Acta* 395 (2002) 225–236.
- [42] H.S. Roh, K.W. Jun, W.S. Dong, J.S. Chang, S.E. Park, Y.I. Joe, *J. Mol. Catal. A: Chem.* 181 (2002) 137–142.
- [43] H.S. Roh, K.W. Jun, S.E. Park, *Appl. Catal. A: Gen.* 251 (2003) 275–283.
- [44] W. Nimwattanakul, A. Luengnaruemitchai, S. Jitkarnka, *Inter. J. Hydrogen Energy* 31 (2006) 93–100.
- [45] W.J. Jang, D.W. Jeong, J.O. Shim, H.S. Roh, I.H. Son, S.J. Lee, *Inter. J. Hydrogen Energy* 38 (2013) 4508–4512.
- [46] S. Li, C. Zhang, Z. Huang, G. Wu, J.A. Gong, *Chem. Commun.* 49 (2013) 4226–4228.
- [47] W.H. Fang, C. Pirez, S. Paul, M. Jiménez-Ruiz, H. Jobic, F. Dumeignil, L. Jalowiecki-Duhamel, *Inter. Hydrogen Energy* 41 (2016) 15443–15452, <http://dx.doi.org/10.1016/j.ijhydene.2016.04.019>.
- [48] M.A. Salam, S. Safian, T. Murugesan, *Chem. Eng. Res. Design* 91 (2013) 2639–2647.
- [49] K. Aika, T. Takano, S. Murata, *J. Catal.* 136 (1992) 126–140.
- [50] S.J. Wang, S.F. Yin, L. Li, B.Q. Xu, C.F. Ng, C.T. Au, *Appl. Catal. B: Environ.* 52 (2004) 287–299.
- [51] S.F. Yin, B.Q. Xu, C.F. Ng, C.T. Au, *Appl. Catal. B: Environ.* 48 (2004) 237–241.
- [52] S.F. Yin, B.Q. Xu, S.J. Wang, C.T. Au, *Appl. Catal. A: Gen.* 301 (2006) 202–210.
- [53] S.F. Yin, B.Q. Xu, W.X. Zhu, C.F. Ng, X.P. Zhou, C.T. Au, *Catal. Today* 93–5 (2004) 27–38.
- [54] G.E.E. Gardes, G.M. Pajonk, S.J. Teichner, *J. Catal.* 33 (1974) 145–148.
- [55] R. Kramer, M. Andre, *J. Catal.* 58 (1979) 287–295.
- [56] A.A. Lemonidou, M.A. Goula, I.A. Vasalos, *Catal. Today* 46 (1998) 175–183.
- [57] A.G. Boudjahem, S. Monteverdi, M. Mercy, M.M. Bettahar, *J. Catal.* 221 (2004) 325–334.
- [58] L. Spenadel, M. Boudart, *J. Phys. Chem.* 64 (1960) 204–207.
- [59] H.L. Gruber, *J. Phys. Chem.* 66 (1962) 48–54.
- [60] R. Wojcieszak, S. Monteverdi, M. Mercy, I. Nowak, M. Ziolek, M.M. Bettahar, *Appl. Catal. A: Gen.* 268 (2004) 241–253.